



Glycerol steam reforming for hydrogen production: Design of Ni supported catalysts

Valentina Nichele^a, Michela Signoretto^{a,*}, Federica Menegazzo^a, Alessandro Gallo^b, Vladimiro Dal Santo^c, Giuseppe Cruciani^d, Giuseppina Cerrato^e

^a Dipartimento di Scienze Molecolari e Nanosistemi, Università Ca' Foscari Venezia, Consorzio INSTM-UR di Venezia, Calle Larga Santa Marta, 2137, 30123 Venezia, Italy

^b Istituto di Scienze e Tecnologie Molecolari-CNR, Via G. Fantoli 16/15, 20138 Milano, Italy

^c Istituto di Scienze e Tecnologie Molecolari-CNR, Via C. Golgi 19, 20133 Milano, Italy

^d Dipartimento di Scienze della Terra, Università di Ferrara, Via Saragat 1, I-44100 Ferrara, Italy

^e Dipartimento di Chimica IFM e NIS – Centro di Eccellenza, Università di Torino, via P. Giuria, 7, 10125 Torino, Italy

ARTICLE INFO

Article history:

Received 27 June 2011

Received in revised form

26 September 2011

Accepted 4 October 2011

Available online 8 October 2011

Keywords:

Hydrogen

Glycerol

Steam reforming

Biodiesel

Nickel

ABSTRACT

In this work the activity of Ni catalysts in hydrogen production by glycerol steam reforming was studied. Moreover the effect of the support (TiO_2 , SBA-15 and ZrO_2) on the catalytic performance of Ni was evaluated. A strong effect of the support on the activity of the samples was detected. The Ni/TiO_2 sample showed negligible activity mainly due to the low strength of anatase to keep nickel in the reduced state. In fact, both incorporation of Ni ions into the nanoanatase lattice and oxidation of the active phase to NiO under operating conditions were observed. A deactivation process was also found with the $\text{Ni}/\text{SBA}-15$ sample while the best results were achieved with the Ni/ZrO_2 catalyst, showing no deactivation. After 20 h, the glycerol conversion was ~72% and the H_2 yield was ~65%. The Ni/ZrO_2 sample was even more active when tested at lower temperatures, although its performance was less stable. On the basis of the experimental results, it was evidenced that the nature of the support affects above all the stability of the active phase. In particular, strong interactions between the metal active phase and the support ensures stability, activity and selectivity of the catalyst in glycerol steam reforming reactions.

© 2011 Elsevier B.V. All rights reserved.

1. Introduction

The last century witnessed the rise of the petroleum-based chemistry and the exploitation of fossil resources for the production of energy and chemicals. Nevertheless the diminishing availability of these resources, together with the environmental issues related to greenhouse gas emissions, renders the birth of a new chemical industry essential.

Hydrogen is considered as the future energy vector [1], because it is clean and carbon-free and it can be used directly by either thermal combustion or converted into electrical energy by means of fuel cells [2]. Currently hydrogen is produced from fossil fuels, so the amount of carbon dioxide formed during its production is the same as that formed by direct combustion of these fuels [3]. To reduce effectively the greenhouse effect and the global warming, hydrogen should be produced from renewable resources. In this context glycerol has emerged as a promising source of hydrogen, because it has a high hydrogen content and it is safe and non toxic [4]; moreover glycerol is the main by-product (approximately 10 wt%)

in biodiesel production from transesterification of vegetable oils extracted from biomass [5], so its employ would be highly desirable for several reasons. First of all, the expected increase in biodiesel production will cause a glut of waste glycerol, whose disposal will rise even further the price of biodiesel itself; it is then essential to find useful applications for this by-product. Besides that, glycerol is a cheap and renewable source of hydrogen, so its employ for hydrogen production would be advantageous from both the economical and environmental point of view.

The steam reforming (SR) of oxygenated compounds is usually affected by the formation of several by-products, thus reducing the selectivity to hydrogen and leading to the formation of coke. The design of a highly selective catalyst is then fundamental.

Many investigations have been published on glycerol reforming, both in the aqueous [6–8] and in the gas phase [9–11], and several metal-supported catalysts have been tested. The most studied metals are Ir [10], Ru [9], Pt [12] and Pd [8]. Nickel is also both highly active and selective in the steam reforming reactions, because of its high capability to break C–C bonds and also to promote the water–gas shift reactions, thus increasing hydrogen production [13,14]. We then decided to use nickel in the preparation of our catalysts, because it is cheaper and more available than noble metals.

* Corresponding author. Tel.: +39 0412348650; fax: +39 0412348517.

E-mail address: miky@unive.it (M. Signoretto).

As for the support, it plays a key role in the steam reforming reactions, affecting in particular the selectivity of the catalyst [15,16]. The ideal support should possess a good chemical and mechanical resistance and a high surface area, in order to favour the dispersion of the active phase [17,18].

Therefore, the aim of the present work is to investigate the effect of the nature of the support on the catalytic performance of nickel in terms of both activity and selectivity in the steam reforming of glycerol.

2. Experimental

2.1. Catalysts preparation

2.1.1. Supports synthesis

TiO_2 was prepared by a conventional precipitation method. 20 g of $\text{TiOSO}_4 \cdot x\text{H}_2\text{SO}_4 \cdot x\text{H}_2\text{O}$ (Aldrich, synthesis grade) were dissolved in 300 mL of distilled water at room temperature, then NaOH (Carlo Erba, 9 M) was added dropwise until the system reached a pH of 5.5. The precipitate was aged at 60 °C for 20 h, then repeatedly washed with distilled water and finally dried overnight at 110 °C.

SBA-15 was synthesized as previously reported [19], in the presence of Pluronic 123 (P123, Aldrich) as structure directing agent.

ZrO_2 was prepared by a conventional precipitation method [20] at a constant pH of 10.

2.1.2. Introduction of the active phase

The active phase was added to each support by incipient wetness impregnation with an aqueous solution of the metallic precursor ($\text{Ni}(\text{NO}_3)_2 \cdot 6\text{H}_2\text{O}$, Sigma-Aldrich, purity ≥98.5%), in the proper concentration in order to obtain the desired Ni loading (10 wt%). The catalyst was dried overnight at 110 °C and then calcined at 500 °C for 4 h.

Samples are identified as Ni/TiO_2 , $\text{Ni}/\text{SBA-15}$ and Ni/ZrO_2 .

2.2. Catalysts characterization

The temperature programmed reduction (TPR) measurements were carried out by placing the catalyst in a quartz reactor and heating in a 5% H_2/Ar mixed gas stream flowing at 40 mL/min at a heating rate of 10 °C/min from 25 to 600 °C. H_2 consumption was monitored with a TCD detector.

Before the other characterization measurements, the samples were reduced in H_2 flow for 1 h at 500 °C and 700 °C (N_2 physisorption) or only at 500 °C (XRD and HR-TEM).

Specific surface area and pores size distribution were evaluated through N_2 adsorption-desorption isotherms at 77 K (MICROMERITICS, ASAP 2000 Analyser). Surface area was calculated on the basis of the BET equation [21], whereas the pores size distribution was determined by the BJH method, applied to the N_2 desorption branch of the isotherm [22]. Prior to the analyses the samples were dried overnight at 110 °C and then outgassed in vacuum at 110 °C for 2 h.

X-ray powder diffraction (XRD) patterns were measured by a Bruker D8 Advance diffractometer equipped with a Si(Li) solid state detector (SOL-X) and a sealed tube providing $\text{Cu K}\alpha$ radiation. The quantitative phase analysis and crystal size determination of the support and metal phases in the samples were obtained by the Rietveld refinement method as implemented in the Bruker TOPAS program.

(High-resolution) Transmission electron microscopy (HR-TEM) images were obtained by using a JEOL JEM 3010UHR (300 kV) TEM fitted with a single crystal LaB_6 filament and an Oxford INCA Energy TEM 200 energy dispersive X-ray (EDX) detector. All samples were dry deposited on Cu "holey" carbon grids (200 mesh).

2.3. Catalytic tests

The activity of Ni catalysts in glycerol steam reforming was evaluated in a fixed-bed quartz reactor (diameter 12 mm) operating at atmospheric pressure and at different temperatures (500 and 650 °C) for 20 h.

Catalytic tests were carried out in a home-made equipment. 200 mg of catalyst sieved to 35–45 mesh were loaded in the reactor and reduced *in situ* at 500 °C (if the reaction was performed at 500 °C) or 700 °C (if the reaction was performed at 650 °C) under hydrogen flow for 1 h prior to the reaction. Then a glycerol (10 wt%)/water solution was fed (0.060 mL/min) by means of a diaphragm metering pump (Stepdos, KNF) and helium was used as carrier gas (30 mL/min); a pressure controller was placed before the inlet gas to prevent overpressure phenomena. Vaporization of the solution took place before the catalytic bed in a unit filled with quartz beads at 250 °C.

The analysis of the gaseous products was carried out by a gas chromatograph (Agilent 6890N) equipped with two columns connected in series (MS and Poraplot Q) with thermal conductivity and flame ionization detectors (TCD-FID), properly calibrated for the detection of CH_4 , CO , CO_2 , H_2 ; condensables were removed through a refrigerated coil.

The steam reforming of glycerol leads to the formation of H_2 and CO_2 according to the reaction $\text{C}_3\text{H}_8\text{O}_3 + 3\text{H}_2\text{O} \rightarrow 7\text{H}_2 + 3\text{CO}_2$. The performance of the catalysts is presented in terms of H_2 yield, C conversion and CO , CH_4 and CO_2 selectivity, calculated from Eqs. (1)–(3):

$$\% \text{H}_2 \text{ yield} = \frac{\text{H}_2 \text{ mol produced}}{(\text{mol glycerol in the feed}) \times 7} \times 100 \quad (1)$$

$$\% \text{C conversion} = \frac{(\text{CO}_2 + \text{CO} + \text{CH}_4) \text{ mol produced}}{3 \times (\text{mol glycerol in the feed})} \times 100 \quad (2)$$

$$\% \text{Selectivity of } i = \frac{i \text{ mol}}{(\sum i \text{ species}) \text{ mol produced}} \times 100 \quad (3)$$

where i represents CO , CO_2 and CH_4 .

3. Results and discussion

Before discussing the experimental results, it can be useful to see in detail how hydrogen production through glycerol steam reforming takes place.



Eq. (4) represents the overall steam reforming reaction, an endothermic transformation favoured at low pressure which is due to the contribution of two reactions, namely glycerol decomposition (Eq. (5)) and water gas shift (WGS, Eq. (6)). The reaction pathway is quite complex and many other reactions can take place, in particular CO and CO_2 hydrogenation, which leads to the formation of methane, and side reactions, such as dehydration, dehydrogenation, cyclization and polymerization, that can lead to coke deposition [23,24].

The activity of the catalysts in the steam reforming of glycerol performed at 500 °C and at 650 °C is reported in Fig. 1; activity is presented in terms of glycerol conversion and hydrogen yield. In Fig. 2 the selectivity to CO and CO_2 is shown.

Fig. 1 shows that Ni/TiO_2 sample exhibits negligible catalytic activity at both temperatures: after 20 h-on-stream, glycerol conversion is lower than 10% and hydrogen yield does not reach 5%. This catalyst has a high selectivity to CO , which is the main carbon product. CO_2 production greatly differs according to the reaction

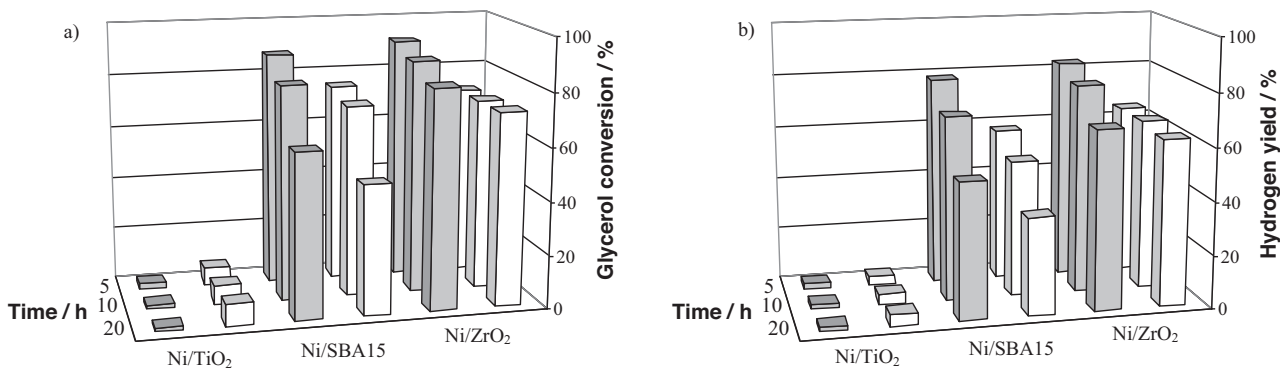


Fig. 1. Catalytic performance of the catalysts in glycerol steam reforming at two different temperatures: ■ 500 °C; □ 650 °C. (a) Glycerol conversion; (b) hydrogen yield.

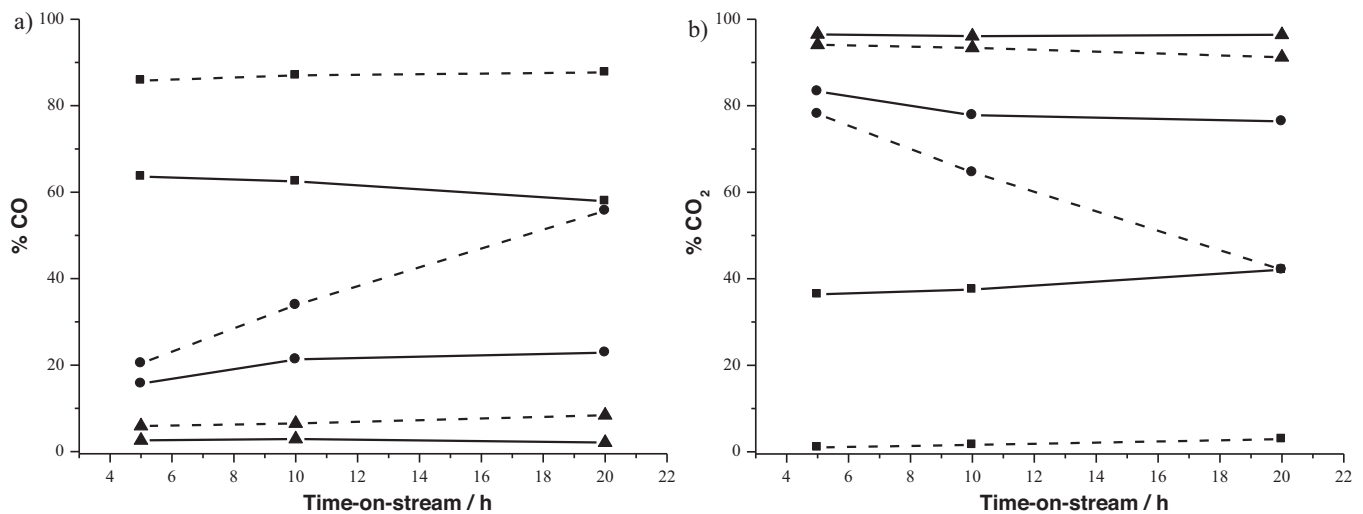


Fig. 2. CO (a) and CO₂ (b) selectivity for Ni/TiO₂ (■), Ni/SBA-15 (●) and Ni/ZrO₂ (▲) at 500 °C (solid line) and 650 °C (dash line).

temperature (see Fig. 2(b)): it is very low at 650 °C, while it is prominent at 500 °C. Moreover, when the reaction is performed at 650 °C, a little amount (~10%) of CH₄ is also present. In the generally accepted mechanism of metal catalysed glycerol steam reforming, the rate determining step is C–C cleavage, which leads to adsorbed CO. Carbon monoxide must be removed from the catalyst surface by the water–gas shift reaction because high surface coverage by CO decreases the catalytic activity [8]. The results obtained for Ni/TiO₂ sample show that this catalyst has a very low activity in C–C bond cleavage, even at the highest temperature, and that the contribution of the water–gas shift reaction is even smaller.

The SBA-15 sample shows the same behaviour at both temperatures (Fig. 1): it has a high initial activity, but it undergoes a deactivation process which decreases the glycerol conversion. At 500 °C, after 20 h-on-stream, a glycerol conversion of 62% and a hydrogen yield of 51% were obtained. CO formation is quite stable in the course of time. At 650 °C glycerol conversion and hydrogen yield are much lower (49% and 37% respectively), while CO production is significant and increases with time.

The Ni/ZrO₂ sample achieved the best performance (Fig. 1); the most relevant difference related to the reaction temperature is that a little deactivation is detected at 500 °C, while a stable glycerol conversion of ~72% and a hydrogen yield of 65% are obtained at 650 °C. In both cases the main carbon product is CO₂: this evidences the important contribution of the water–gas shift reaction that consumes CO and increases H₂ production even further.

The origin of the differences in the catalytic behaviour of the samples can be discussed on the basis of the characterization measurements we carried out.

First of all we carried out TPR measurements (Fig. 3), in order to identify the different NiO species on the surface of the supports and their reduction temperature.

It is possible to note that three different NiO species are present on the samples. The TPR pattern of the Ni/TiO₂ sample shows a broad reduction region, in the range 290–500 °C; three different peaks at 370 °C, 410 °C and 450 °C can be detected. The TPR profile of the SBA-15 sample is quite broad too: a well-defined peak with its maximum at 390 °C, a shoulder between 300 and 360 °C and

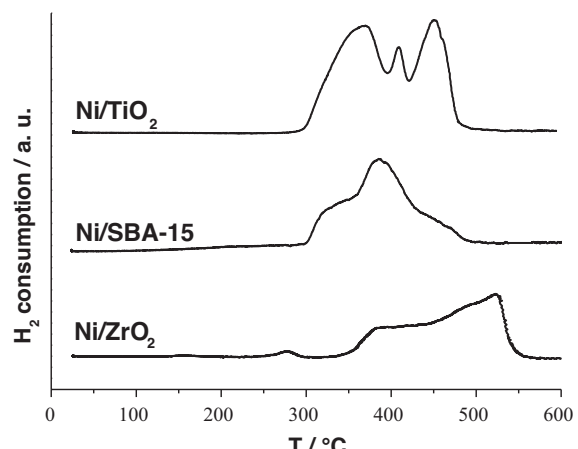


Fig. 3. TPR profiles of the catalysts.

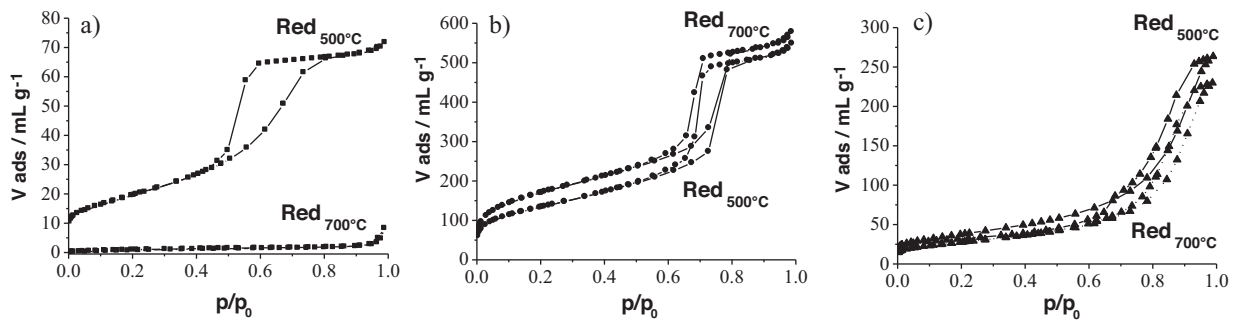


Fig. 4. N_2 adsorption/desorption isotherms of Ni/TiO_2 (a), $\text{Ni}/\text{SBA-15}$ (b) and Ni/ZrO_2 (c) after reduction of the samples.

another one between 420 and 500 °C are present. Lastly Ni/ZrO_2 TPR reveals three peaks at 280 °C, 380 °C and 520 °C.

The peak located at the lowest temperature is ascribable to non-interacting metal oxide particles, more easily reduced (unsupported NiO has a reduction temperature of about 280 °C [25]). The other two peaks can be assigned to NiO particles weakly (peak at a lower temperature) or strongly (peak at a higher temperature) interacting with the support [26–30]. It can be noted that the position of the peaks differs according to the nature of the support.

All the catalysts are completely reduced within 550 °C and strong interactions between Ni and the support exist in all the samples. A relevant percentage of non-interacting Ni particles is present on the TiO_2 sample.

One of the most important parameters in the design of heterogeneous catalysts is the specific surface area: in fact, it is well known that a high surface area greatly improves the dispersion of the active phase [31,32]. The specific surface area (Fig. 4) was evaluated after reduction of the samples at 500 °C and at 700 °C, thus reproducing the reduction treatment performed before the catalytic tests.

Concerning SBA-15 and ZrO_2 samples, it is quite evident that the reduction temperature does not affect the structure of the materials, which has been preserved in both cases. According to IUPAC classification [33], $\text{Ni}/\text{SBA-15}$ sample (Fig. 4(b)) shows a IV-type isotherm with a H1-type hysteresis, which is typical of this support, a mesoporous material with a high surface area of about 600 m^2/g and a sharp pores size distribution with a maximum at 6 nm, whereas Ni/ZrO_2 sample (Fig. 4(c)) exhibits a IV-type isotherm containing a H3-type hysteresis, typical of materials that do not possess a well-defined mesoporous structure, and a surface area of approximately 100 m^2/g .

The behaviour of the TiO_2 sample is completely different. It can be noted that the Ni/TiO_2 sample (Fig. 4(a)), after reduction at 500 °C, shows a IV-type isotherm, which is typical of mesoporous materials characterized by a quite high surface area and an unimodal pores size distribution; the high temperature (700 °C) reduction treatment, on the contrary, caused the collapse of the porous structure of the oxide and the decrease of the specific surface area from 70 m^2/g to 4 m^2/g .

Physisorption measurements seem to suggest a plausible explanation of the negligible activity of Ni/TiO_2 in the reaction performed at 650 °C, whereas an exhaustive study of the other samples is still necessary. X-ray diffraction measurements were carried out on both the non-reduced and the reduced samples.

XRD patterns taken after the heat treatment in air (data not reported here for the sake of brevity) showed the occurrence of NiO (bunsenite) in both the $\text{Ni}/\text{SBA-15}$ and Ni/ZrO_2 samples, whereas in the case of Ni/TiO_2 only nanocrystalline anatase was found. This result led us to believe that all nickel had been incorporated in the anatase lattice, thus making Ni unavailable to the reaction. This interpretation is in agreement with previous reports in which sol-gel prepared Ni-doped TiO_2 nanoparticles or films heated in

air at 450 °C or 500 °C did not show any Ni phase not only for Ni ion concentration up to 2 mol% in the 0–2 mol% doping range [34] or up to 8 mol% in a doping range 0–10 mol% [35] but even when Ni was as high as 10 mol% [36]. In all these cases the diffraction peaks of doped anatase do not show any detectable shift compared to the undoped sample. Based on this consideration and the closer similarity of Ni^{3+} ionic radii (60 pm) to Ti^{4+} ions (60.5 pm), compared to Ni^{2+} (69 pm), it is likely that Ni ions are incorporated in the higher oxidation state according to a mechanism of 2 Ni^{3+} coupled to an oxygen vacancy as previously documented [37].

The high 2θ angle region of the XRD profile for the reduced TiO_2 sample (Fig. 5(a)) shows that anatase is the main phase of the sample (~10% is brookite). The two peaks at $2\theta \sim 44.5^\circ$ and 51.8° reveal the occurrence of metallic nickel but its content, calculated by detailed Rietveld quantitative phase analysis, is much lower than the effective Ni concentration. This could be due, as reported above, to Ni incorporation in the support, *i.e.* to its lower availability to be reduced in H_2 flow. We then suppose that the little fraction of metallic nickel is not sufficient to catalyse the steam reforming reaction and that this could be the reason for its low activity. For what concerns the SBA-15 sample, the low angle XRD pattern of SBA-15 (Fig. 5(b)) is characterized by the presence of a prominent peak located at $2\theta \sim 0.8^\circ$ and of another weak peak at $2\theta \sim 1.8^\circ$: they can be ascribed to the (1 0 0) and (1 1 0) diffractions, respectively, associated with the 2-D p6 mm hexagonal symmetry. The peaks at $2\theta \sim 44.5^\circ$ and 51.8° correspond to metallic Ni. Finally, in the XRD profile of the ZrO_2 sample (Fig. 5(c)) only a tetragonal phase is observed and, also in this case, the presence of metallic Ni (peaks at $2\theta \sim 44.5^\circ$ and 51.8°).

We then carried out the transmission electron microscopy (HR-TEM) investigation on both fresh and exhausted catalysts in order to follow the evolution and/or transformation of the samples under the reaction conditions, thus explaining their catalytic performances.

Fig. 6(a) shows that the support of the reduced TiO_2 sample before the reaction is made up of a highly crystalline titanium dioxide, as confirmed by the high incidence of fringes patterns, generated by the presence of crystalline planes exhibiting low hkl indexes. In particular, the inspection in detail of the spacing ($d = 0.357 \text{ nm}$) among the interference fringes indicates that the most preferentially exposed planes belong to the (1 0 1) TiO_2 anatase polymorph. Moreover, the dispersion of Ni particles on titania is very high: an average nanoparticles dimension of about 0.5 nm has been estimated (see the 10 \times blown-up section of Fig. 6(a)).

EDS (energy dispersive X-ray spectroscopy) measurements demonstrated the presence of Ni (spectra not reported for the sake of brevity). These results are in agreement with XRD data and confirm the presence of Ni species on the surface but, apparently, in a too low concentration.

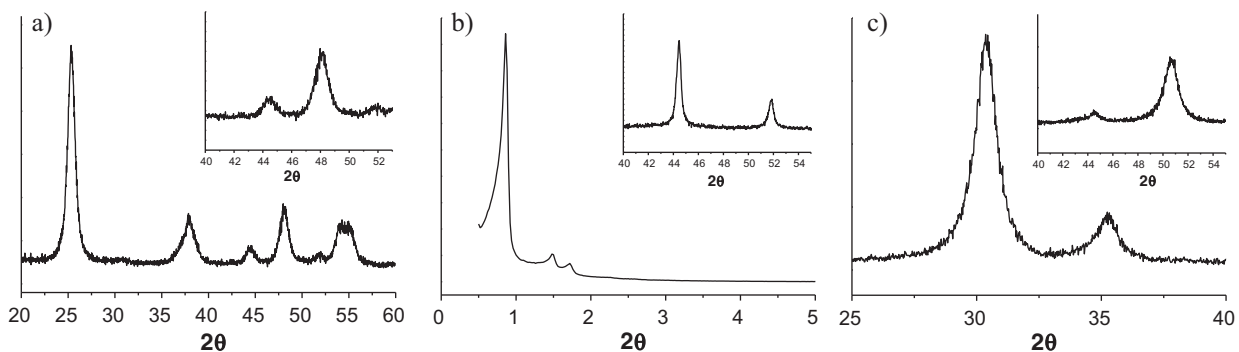


Fig. 5. XRD profiles of Ni/TiO₂ (a), Ni/SBA-15 (b) and Ni/ZrO₂ (c); Ni peaks at $2\theta \sim 44.5^\circ$ and $2\theta \sim 52^\circ$ (insets).

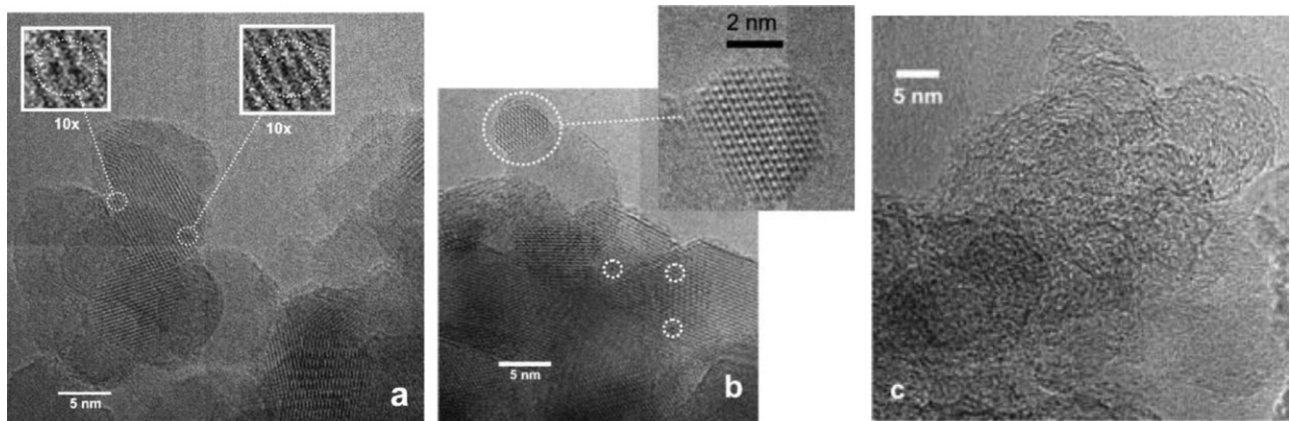


Fig. 6. TEM images of Ni/TiO₂ sample: fresh Ni/TiO₂ (a), Ni/TiO₂ after SR at 500 °C (b), Ni/TiO₂ after SR at 650 °C (c).

Moreover, TEM measurements relative to the corresponding exhausted sample (SR at 500 °C; see Fig. 6(b)) reveal that, in these reaction conditions, the TiO₂ support remains almost unchanged, whereas Ni species are present both as individual metallic particles and also in a partial oxidized form. In fact, the detailed inspection of the fringe patterns indicates that the particles are here and there made up of NiO ($d_{hkl} = 0.208$ nm) and the most exposed crystal planes belong to the (2 0 0) face of NiO (ICDD-PDF file n. 47-1049); see the inset of Fig. 6(b).

Ni oxidation is one of the most common deactivation phenomena of Ni-based catalysts [38]. Nickel can be oxidized by gaseous oxygen, but even by steam at low temperature, as reported by Liberatori et al. [39], and Ni in the oxide form is inactive in steam reforming reactions. A possible explanation of this phenomenon could be the low interactions between the metal and the support, as suggested by TPR measurements, which cannot stabilize the metal phase. It has been demonstrated that Ni activity can be increased through the addition of small amounts of noble metals, which can stabilize the Ni sites in the reduced state [40]. Another possibility is to strengthen the interactions of Ni with the support (SMSI) by increasing the calcination temperature. It is well known that at high temperatures NiO and TiO₂ interdiffuse leading to the formation of an ilmenite type structure (NiTiO₃) [41]; Zhang et al. established that nickel in NiTiO₃ is still reducible to Ni⁰ (although at higher temperatures than NiO) and active in the partial oxidation of methane [42]. In the light of these experimental evidences, we decided to prepare a new Ni/TiO₂ sample and calcined it at 800 °C. By XRD we observed that the metal phase was present mainly as NiTiO₃ (see Fig. 7) and that this sample was highly active in glycerol steam reforming, with total glycerol conversion and a selectivity to hydrogen of about 90% (data not shown).

The small amount of metallic Ni available, together with its oxidation in the SR conditions, is then likely to be the reason why, though its high dispersion, this sample is almost entirely inactive in glycerol steam reforming. Some metal particles (of almost unchanged dimensions: see the white circled portions in Fig. 6(b)) can be still detected on the support: they are probably responsible for the very low conversion obtained with this sample (see Fig. 1).

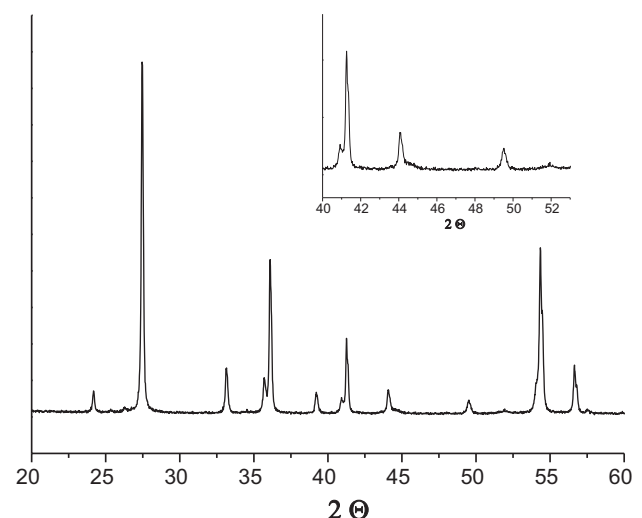


Fig. 7. XRD profile of Ni/TiO₂ calcined at 800 °C; Ni peaks at $2\theta \sim 44.5^\circ$ and $2\theta \sim 52^\circ$ (inset).

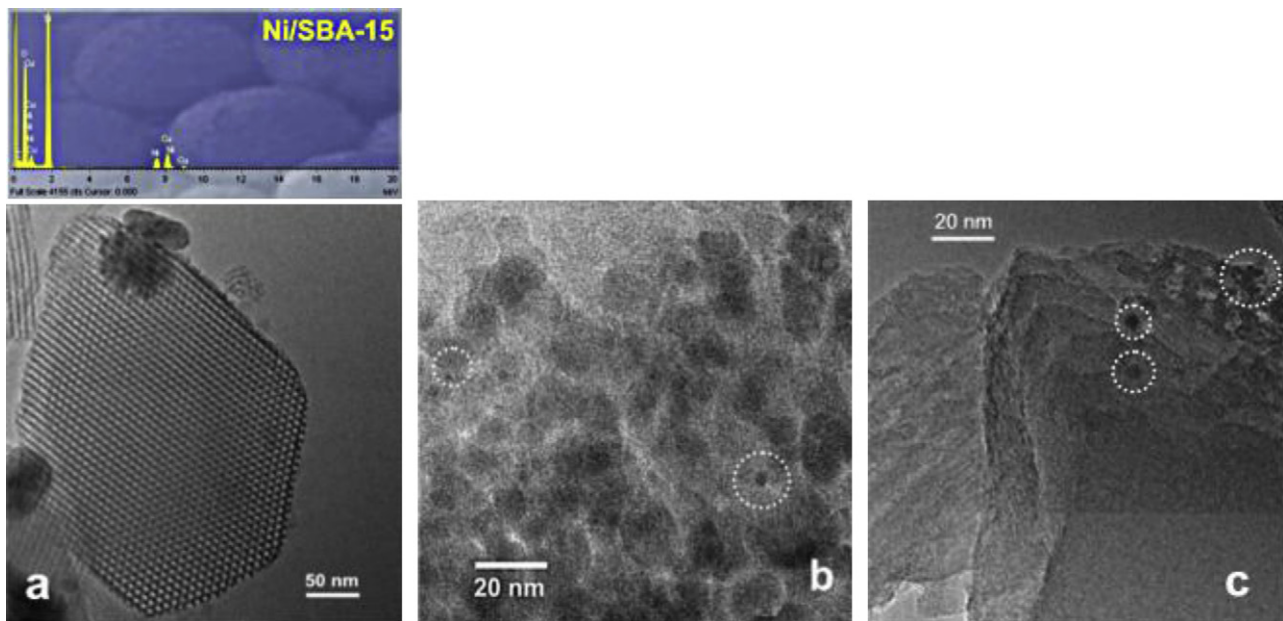


Fig. 8. TEM images of Ni/SBA-15 sample: fresh Ni/SBA-15 (a), Ni/SBA-15 after SR at 500 °C (b), Ni/SBA-15 after SR at 650 °C (c).

Concerning the exhausted catalyst at 650 °C, TEM micrographs (Fig. 6(c)) show that the support is now very hardly observable, as it turns out to be almost totally covered by a thin and amorphous overlayer (coating). The X-ray diffraction pattern (not reported) showed that the almost complete conversion of anatase to rutile, due to the higher reduction temperature, promoted the shift of Ni towards the surface (thus increasing its availability to the reaction), but the collapse of the surface area of the support (revealed also by N₂ physisorption analysis; see Fig. 4(a)) caused the sintering of the active phase (Ni particles diameter of about 50 nm).

As for the Ni/SBA-15 system, TEM images (reported in Fig. 8) of the fresh sample show that in the support it is possible to observe a highly ordered structure with a hexagonal array of cylindrical pores, thus corroborating both physisorption and XRD data. It is quite difficult to detect Ni nanoparticles, although Ni presence has been ascertained by EDS (see the spectrum reported in section 8 (a)). This result seems to suggest that Ni nanoparticles are located mainly within the pores of the support; this hypothesis is further supported by the decrease (about 20%) of the specific surface area of pure SBA-15 after the introduction of the metal phase.

The morphological features reported in Fig. 8(b) and (c) indicate the possible reason of the fast deactivation that occurs for this

sample in glycerol steam reforming at both temperatures, as the SBA-15 mesostructure is gradually destroyed. This is probably due to the poor mechanical and hydrothermal stability of this material: its strength in water steam at high temperatures is known to be too low. The decrease in the catalytic activity can be then ascribed to the collapse of the pore walls, which renders the Ni nanoparticles, located inside the matrix, inaccessible to reagent molecules; the residual observed activity is due to Ni particles exposed on the surface. Many efforts have been spent in order to increase the hydrothermal stability of mesoporous silicas, such as addition of inorganic salts during the synthesis or incorporation of metal oxides, as well as the increase of calcination temperature [43]. Once again, the key role of the support in stabilizing the metal phase has been evidenced.

As for the third catalytic system, Fig. 9(a) reports a TEM image relative to the fresh Ni/ZrO₂ sample, which achieved the best performance in terms of both H₂ yield and stability. As far as the support is concerned, the detailed analysis of the fringe patterns indicates the presence of the tetragonal polymorph of ZrO₂ ($d_{hkl} = 0.296 \text{ nm}$; (111) face; ICDD PDF file n. 79-1763) with an average dimension of the particles of the support of 5–8 nm. Moreover, as for the Ni/TiO₂ sample, the dispersion of Ni particles on

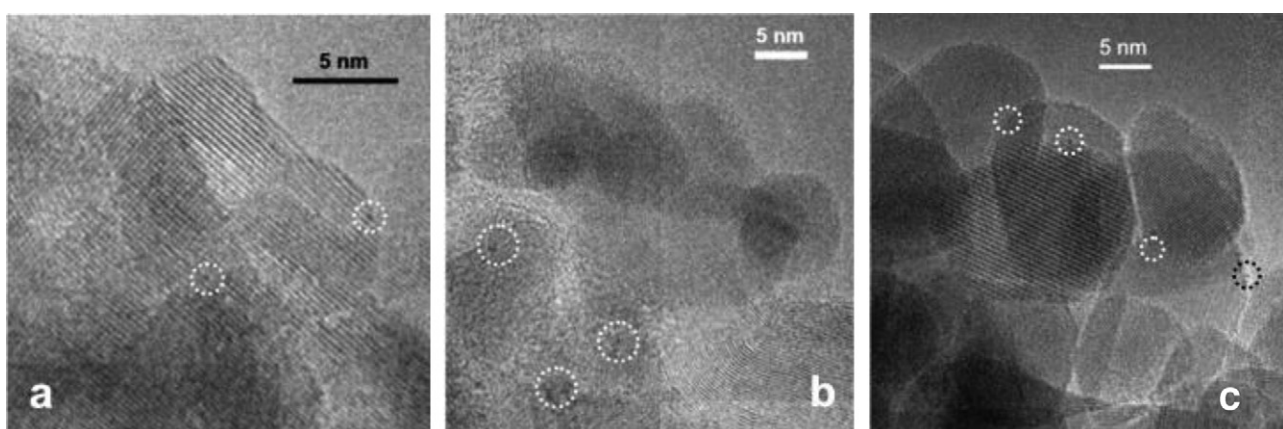


Fig. 9. TEM images of Ni/ZrO₂ sample: fresh Ni/ZrO₂ (a), Ni/ZrO₂ after SR at 500 °C (b), Ni/ZrO₂ after SR at 650 °C (c).

the support is very high and a nanoparticles dimension of about 0.5 nm has been estimated; once again, EDS measurements (not reported for the sake of brevity) ensured that Ni is present. Fig. 9(b) and (c) clearly explain the reason of the excellent catalytic performance maintained by this material: the structure of the zirconia support is fully preserved even after 20 h in the SR conditions, as well as the dispersion of the active phase (Ni nanoparticles dimension remained unchanged).

It has been demonstrated that zirconia improves both thermal stability and oxygen storage capacity, which favours carbon gasification [44]: this study confirms the high capability of zirconia to stabilize the active phase, and this is probably due to the strong interactions between Ni and zirconia, as also highlighted by TPR measurements too (see Fig. 3). Moreover, zirconia is known to possess the ability to first adsorb and then dissociate water, thus enhancing the adsorption of steam on its surface and activating the gasification of hydrocarbons in the SR reactions [16] and the water–gas shift [45].

However, TEM of the Ni/ZrO₂ sample tested at 500 °C evidenced the presence of coke, that could be the cause of the slight deactivation of this sample, although TGA analysis did not reveal an appreciable amount of deposited carbon. On the contrary, no coke formation was detected on the sample tested at 650 °C, whose performance is stable during all the catalytic experiment. It is well known that, among the other parameters (*i.e.*, pressure or water to glycerol molar ratio), temperature plays a key role in glycerol steam reforming. Taking into account the reaction pathways, from the thermodynamic point of view the steam reforming reaction is favoured at high temperature, whereas the water–gas shift reaction is favoured at low temperature. This is the reason why the Ni capability to break C–C bonds at low temperatures is lower and secondary reactions (dehydration, rearrangement and condensation) are favoured, leading to the formation of unsaturated compounds which are good precursors in coke deposition. Our results seem to suggest that at 500 °C Ni activity in glycerol SR is too low to prevent the formation of both by-products and coke, whereas it is possible to obtain hydrogen with high selectivity at 650 °C.

Ni/ZrO₂ catalyst proved to be an excellent catalyst for glycerol steam reforming; an optimization of the reaction conditions should be carried on to increase its performance even further.

4. Conclusions

In this work we demonstrated the suitability of Ni-based catalysts to be used in glycerol steam reforming, due to Ni activity in breaking C–C bonds and also in promoting the water–gas shift reaction. In particular, the present work highlights the importance of the nature of the support, because it has been demonstrated to play a key role in designing the catalytic performance. According to our results, the support affects the stability of the active phase above all: as a consequence, the catalytic performance itself greatly depends on the reaction conditions. In particular we reported that strong metal–support interactions ensures stability, activity and selectivity of the catalyst in glycerol steam reforming.

We demonstrated that SBA-15 system possesses an insufficient hydrothermal resistance, which is responsible for the progressive deactivation of the catalyst, although it stabilizes the active phase in an efficient way, thus preventing sintering. On the other hand, the titania support favours the oxidation and incorporation of Ni ions into the anatase lattice upon heating in air. After treatment under H₂ flow at least a fraction on Ni is reduced to metallic particles. However, anatase is stable only at relatively low temperatures and its weak interactions with Ni cannot prevent the oxidation (*i.e.* inactivation) of the active phase in the SR conditions. Finally, zirconia system proved to be the best support for Ni in the steam

reforming of glycerol because it possesses all the necessary features: high surface area, high stability in the reaction conditions, strong interactions with the metal phase. Moreover a strong effect of temperature has been detected: it is noteworthy that glycerol conversion at 650 °C is stable, with no deactivation and a high and stable hydrogen production. Ni/ZrO₂ catalyst seems to be very promising and its performance could be improved even further by properly tuning the operational conditions.

Acknowledgements

The financial support of Regione Lombardia (project “M4H2 – Materiali innovativi per la produzione di H₂ da fonti rinnovabili”), Regione Lombardia – INSTM (RU of Venice) and CNR Milano; Italian MIUR (Project “ItalNanoNet”) is gratefully acknowledged.

References

- [1] J.A. Calles, A. Carrero, A.J. Vizcaíno, *Micropor. Mesopor. Mater.* 119 (2009) 200–207.
- [2] M. Benito, R. Padilla, L. Rodríguez, J.L. Sanz, L. Daza, *J. Power Sources* 169 (2007) 167–176.
- [3] S. Czernik, R. French, C. Feik, E. Chornet, *Ind. Eng. Chem. Res.* 41 (2002) 4209–4215.
- [4] F. Pompeo, G. Santori, N.N. Nichio, *Int. J. Hydrogen Energy* 35 (2010) 8912–8920.
- [5] M.J. Haas, A.J. McAlloon, W.C. Yee, T.A. Foglia, *Bioresour. Technol.* 97 (2006) 671–678.
- [6] J.W. Shabaker, R.R. Davda, G.W. Huber, R.D. Cortright, J.A. Dumesic, *J. Catal.* 215 (2003) 344–352.
- [7] J.W. Shabaker, G.W. Huber, J.A. Dumesic, *J. Catal.* 222 (2004) 180–191.
- [8] G.W. Huber, J.W. Shabaker, S.T. Evans, J.A. Dumesic, *Appl. Catal. B: Environ.* 62 (2006) 226–235.
- [9] T. Hirai, N. Ikenaga, T. Miyake, T. Suzuki, *Energy Fuels* 19 (2005) 1761–1762.
- [10] B. Zhang, X. Tang, Y. Li, Y. Xu, W. Shen, *Int. J. Hydrogen Energy* 32 (2007) 2367–2373.
- [11] S. Adhikari, S.D. Fernando, S.D. Filip To, R.M. Bricka, P.H. Steele, A. Haryanto, *Energy Fuels* 22 (2008) 1220–1226.
- [12] A.O. Menezes, M.T. Rodrigues, A. Zimmaro, L.E.P. Borges, M.A. Fraga, *Renew. Energy* 36 (2011) 595–599.
- [13] R.R. Davda, J.W. Shabaker, G.W. Huber, R.D. Cortright, J.A. Dumesic, *Appl. Catal. B: Environ.* 43 (2003) 13–26.
- [14] R.R. Davda, J.W. Shabaker, G.W. Huber, R.D. Cortright, J.A. Dumesic, *Appl. Catal. B: Environ.* 56 (2005) 171–186.
- [15] G. Wen, Y. Xu, H. Ma, Z. Xu, Z. Tian, *Int. J. Hydrogen Energy* 33 (2008) 6657–6666.
- [16] M.H. Youn, J.G. Seo, H. Lee, Y. Bang, J.S. Chung, I.K. Song, *Appl. Catal. B: Environ.* 98 (2010) 57–64.
- [17] A. Iriondo, V.L. Barrio, J.F. Cambra, P.L. Arias, M.B. Guemez, M.C. Sanchez-Sánchez, R.M. Navarro, J.L.C. Fierro, *Int. J. Hydrogen Energy* 35 (2010) 11622–11633.
- [18] M. Lindo, A.J. Vizcaíno, J.A. Calles, A. Carrero, *Int. J. Hydrogen Energy* 35 (2010) 5895–5901.
- [19] E. Ghedini, M. Signoretto, F. Pinna, G. Cruciani, *Catal. Lett.* 125 (2008) 359–370.
- [20] F. Zane, S. Melada, M. Signoretto, F. Pinna, *Appl. Catal. A: Gen.* 299 (2006) 137–144.
- [21] S. Brunauer, P.H. Emmett, E. Teller, *J. Am. Chem. Soc.* 60 (1938) 309–319.
- [22] E.P. Barrett, L.G. Joyner, P.P. Halenda, *J. Am. Chem. Soc.* 73 (1951) 373–380.
- [23] C.K. Cheng, S.Y. Foo, A.A. Adesina, *Ind. Eng. Chem. Res.* 49 (2010) 10804–10817.
- [24] V. Chioldo, S. Freni, A. Galvagno, N. Mondello, F. Frusteri, *Appl. Catal. A: Gen.* 381 (2010) 1–7.
- [25] L. Zhang, J. Lin, Y. Chen, *J. Chem. Soc., Faraday Trans.* 88 (1992) 2075–2078.
- [26] Y.Q. Song, D.H. He, B.Q. Xu, *Appl. Catal. A: Gen.* 337 (2008) 19–28.
- [27] V. García, J.J. Fernández, W. Ruiz, F. Mondragón, A. Moreno, *Catal. Commun.* 11 (2009) 240–246.
- [28] M.J. Lazar, Y. Echegoyen, C. Alegre, I. Suelves, R. Moliner, J.M. Palacios, *Int. J. Hydrogen Energy* 33 (2008) 3320–3329.
- [29] B. Huang, X. Li, S. Ji, B. Lang, F. Habimana, C. Li, *J. Nat. Gas Chem.* 17 (2008) 225–231.
- [30] S. Ren, P. Zhang, H. Shui, Z. Lei, Z. Wang, S. Kang, *Catal. Commun.* 12 (2010) 132–136.
- [31] F. Pinna, *Catal. Today* 41 (1998) 129–137.
- [32] A. Taguchi, F. Schüth, *Micropor. Mesopor. Mater.* 77 (2005) 1–45.
- [33] IUPAC. Recommendations, *Pure Appl. Chem.* 57 (1985) 603–619.
- [34] D. Zhang, *J. Sol-Gel Sci. Technol.* 58 (2011) 312–318.
- [35] P. Guo, L. Guo, in: D. Stolten, T. Grube (Eds.), 18th World Hydrogen Energy Conference 2010 – WHEC 2010 – Parallel Sessions Book 3: Hydrogen Production Technologies – Part 2, Proceedings of the WHEC, May 16–21, 2010, Essen – Schriften des Forschungszentrums Jülich/Energy & Environment, vol. 78-3, Institute of Energy Research – Fuel Cells (IEF-3) – Forschungszentrum Jülich GmbH, Zentralbibliothek, Verlag, 2010.

- [36] S.D. Sharma, D. Singh, K.K. Saini, C. Kant, V. Sharma, S.C. Jain, C.P. Sharma, *Appl. Catal. A: Gen.* 314 (2006) 40–46.
- [37] J. Chen, G.-H. Lu, H. Cao, T. Wang, Y. Xu, *Appl. Phys. Lett.* 93 (2008) 172504–172506.
- [38] K. Takehira, T. Ohi, T. Miyata, M. Shiraga, T. Sano, *Top. Catal.* 42–43 (2007) 471–474.
- [39] J.W.C. Liberatori, R.U. Ribeiro, D. Zanchet, F.B. Noronha, J.M.C. Bueno, *Appl. Catal. A: Gen.* 327 (2007) 197–204.
- [40] L.P.R. Profeti, E.A. Ticianelli, E.M. Assaf, *Int. J. Hydrogen Energy* 34 (2009) 5049–5060.
- [41] P.K. de Bokx, R.L.C. Bonne, J.W. Geus, *Appl. Catal.* 30 (1987) 33–46.
- [42] Y. Zhang, Z. Li, X. Wen, Y. Liu, *Chem. Eng. J.* 121 (2006) 115–123.
- [43] E.B. Celer, M. Kruk, Y. Zuzek, M. Jaroniec, *J. Mater. Chem.* 16 (2006) 2824–2833.
- [44] I.N. Buffoni, F. Pompeo, G.F. Santori, N.N. Nichio, *Catal. Commun.* 10 (2009) 1656–1660.
- [45] K.G. Azzam, I.V. Babich, K. Seshan, L. Lefferts, *J. Catal.* 251 (2007) 153–162.